Computational Study of Tin-Catalyzed Baeyer−Villiger Reaction Pathways Using Hydrogen Peroxide as Oxidant

Robert R. Sever and Thatcher W. Root*

Department of Chemical Engineering, University of Wisconsin−Madison, 1415 Engineering Drive, Madison, Wisconsin 53706

Received: February 8, 2003; In Final Form: June 28, 2003

Density functional theory has been used to study several possible reaction mechanisms for tin-catalyzed Baeyer−Villiger oxidation of the model ketone acetone with hydrogen peroxide. The tin catalyst has been modeled with unconstrained single coordination sphere clusters using a B3LYP/ECP methodology. The Baeyer−Villiger reaction mechanism involves two principal steps: (1) addition of the hydrogen peroxide oxidant and the ketone substrate to form the Criegee intermediate and (2) Baeyer−Villiger rearrangement of the Criegee intermediate to yield the ester product. The Gibbs activation barriers for the addition and rearrangement steps in the noncatalyzed mechanism are 39.8 and 41.7 kcal/mol, respectively. In the absence of solvent coordination, tin activates hydrogen peroxide to produce a tin hydroperoxo (SnOOH) intermediate with a Gibbs activation barrier of 15.4 kcal/mol. Water molecules coordinating the tin active site facilitate proton transfer and lower the Gibbs activation barrier for tin hydroperoxo intermediate formation by 3−7 kcal/mol. The tin-catalyzed Baeyer−Villiger mechanism proceeds through a Criegee intermediate that contains a five-membered chelate ring with the tin center. This intermediate can be generated via two degenerate reaction pathways, one of which involves participation of the tin hydroperoxo intermediate. The Gibbs activation barriers for chelated Criegee intermediate formation are less than 14 kcal/mol. Rearrangement of the chelated Criegee intermediate is the rate-determining step for the tin-catalyzed Baeyer−Villiger mechanism. The Gibbs activation barrier for rearrangement is 24.1 kcal/mol when tin possesses no ligands and 21.4 kcal/mol when a single water ligand coordinates tin. The Lewis acidic tin center assists departure of the hydroxyl leaving group in the transition state for Baeyer−Villiger rearrangement. Increased branching of the migrating α carbon in the ketone substrate reduces the activation barrier for the rate-determining rearrangement step by promoting nucleophilic attack of the peroxo bond.

Introduction

The Baeyer−Villiger reaction is the oxidation of a ketone to an ester or lactone by a hydroperoxide (Figure 1). Esters and lactones are important intermediates and products in a wide range of industries, including the agrochemical, dyestuff, flavor, fragrance, pharmaceutical, and polymer industries. Baeyer−Villiger oxidation is a prominent reaction in synthetic organic chemistry due to its versatility and highly predictable regioselectivity and stereoselectivity. Several excellent reviews on the subject are available.[1−4]

Baeyer−Villiger oxidations traditionally have been performed with peroxycarboxylic acids as oxidants, but it is becoming increasingly recognized that such oxidants are problematic for industrial scale use. They generate stoichiometric amounts of carboxylic acid waste as coproduct, which necessitates additional costly process steps to recycle the acid and regenerate the active oxidant. The acid coproduct can also catalyze unwanted side reactions and thereby decrease ester selectivities. Many peroxycarboxylic acids are capable of oxidizing a wide array of functional groups. This capability can be detrimental for achieving chemoselective oxygenation of the complex, multifunctional substrates often used in the industries mentioned above. Two of the most active peroxycarboxylic acids, *m*-chloroperbenzoic acid and trifluoroperacetic acid, can be unstable in solution and typically require chlorinated solvents for optimum performance.

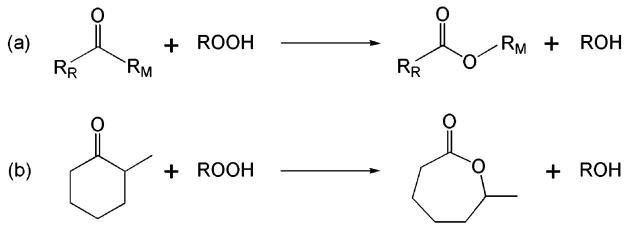

Figure 1. General Baeyer−Villiger oxidation of (a) an acyclic ketone to an ester and (b) a cyclic ketone to a lactone.

Hydrogen peroxide avoids many of the problems associated with peroxycarboxylic acids. Hydrogen peroxide is environmentally friendly because it generates water as the only coproduct of its reduction. It is also commercially available, inexpensive, and easy to handle. The economic advantage of hydrogen peroxide is especially apparent in cases where the conventional peroxycarboxylic acid oxidants are directly prepared from hydrogen peroxide. Hydrogen peroxide contains a higher concentration of active oxygen (47 wt %) than all other oxidants except molecular oxygen. The higher active oxygen content not only improves process economics from the vantage of reactant costs but also leads to lower effluent outputs. Despite these advantages of hydrogen peroxide, its direct use as oxidant

* Corresponding author. E-mail: thatcher@engr.wisc.edu.

10.1021/jp034332c CCC: $25.00
Published on Web 09/06/2003

has been limited because it requires a catalyst for sufficient activity and selectivity in most partial oxidation reactions.

A number of different catalysts have been proposed to accomplish Baeyer−Villiger oxidation with hydrogen peroxide. Because acids are known to catalyze Baeyer−Villiger oxidations with peroxycarboxylic acids, several attempts have been made to use either homogeneous Brønsted acids[5−7] or heterogeneous solid acids[8−12] as catalysts for hydrogen peroxide. The mechanism of acid catalysis can involve either in situ formation of peracids or protonation of reactants or intermediates. The main drawback of acid catalysis is that acids also catalyze unwanted side reactions. Enzymatic Baeyer−Villiger oxidations with molecular oxygen often employ flavin moieties as cofactors.[13] It has been found that flavin species in isolation also show some limited activity as organocatalysts for Baeyer−Villiger oxidations with hydrogen peroxide.[14,15] Most research efforts have focused on developing Lewis acid catalysts that can activate either the ketone carbonyl or the peroxide oxidant.[4,16−32] A variety of Lewis acidic transition metal complexes have been tested as homogeneous Baeyer−Villiger catalysts.[4,16−22] Most show only limited activity or selectivity. The most promising homogeneous catalysts are the Pt(II) diphosphine hydroxy complexes developed by Strukul and co-workers;[17,18] however, they lose much of their activity when anchored on polymer supports.[23]

Other potential heterogeneous Baeyer−Villiger catalysts can be created by incorporating a Lewis acidic metal into the framework of a molecular sieve. Only titanium- and tin-containing redox molecular sieves have been tested for Baeyer−Villiger oxidation with hydrogen peroxide.[24−27] Bhaumik et al.[24] reported that titanium silicalite-1 (TS-1) catalyzes the oxidation of cyclohexanone and acetophenone with hydrogen peroxide under biphase or triphase reaction conditions, but the activity and ester selectivity were low for all cases. Corma and co-workers[25,26] recently announced that tin-containing β zeolite (Sn-β) is a highly active and chemoselective catalyst for Baeyer−Villiger oxidations with hydrogen peroxide. Sn-β is almost 1 order of magnitude more active than the homogeneous platinum complexes of Strukul and co-workers,[17] and selectivities for saturated and unsaturated cyclic ketones with Sn-β are greater than 98%. Ti-β, on the other hand, demonstrated approximately 20 times less activity than Sn-β for the Baeyer−Villiger oxidation of cyclohexanone and exclusively catalyzed epoxidation in preference to Baeyer−Villiger oxidation when tested with the unsaturated cyclic ketone dihydrocarvone.[26] On the basis of these results, Corma et al.[25] proposed a mechanism in which coordination of the ketone substrate on the Lewis acidic tin sites activates the carbonyl group for reaction with free hydrogen peroxide. According to this proposal, tin does not activate the hydrogen peroxide oxidant and thereby avoids epoxidation of unsaturated ketones. Later results with Sn-MCM-41 catalysts show that tin does not exclusively activate the carbonyl moiety.[27] The reaction of dihydrocarvone with hydrogen peroxide in the presence of Sn-MCM-41 yielded lactones with only 68% selectivity, and most side products originated from epoxidation of the double bond. In the wake of the Sn-β discovery, Pillai and Sahle-Demessie[28] have shown that tin-containing hydrotalcites are also active catalysts for Baeyer−Villiger oxidation with hydrogen peroxide. Tin-containing redox molecular sieves and hydrotalcites are environmentally advantageous catalysts not only because they activate hydrogen peroxide but also because their heterogeneous nature enables facile catalyst recovery and recycling. Furthermore, any tin leached from these catalysts will probably take the form of inorganic tin oxides that pose little environmental threat.

Despite the industrial and academic importance of the Baeyer−Villiger reaction, relatively few computational studies of its mechanism have been published. Most of these studies have focused on Baeyer−Villiger oxidations with peroxycarboxylic acids as oxidants.[33−39] To the best of our knowledge, only one computational study of the Baeyer−Villiger reaction with hydrogen peroxide has been reported. Carlqvist et al.[40] investigated noncatalyzed and BF_3-catalyzed mechanisms for Baeyer−Villiger oxidation of acetone with hydrogen peroxide using ab initio and density functional theory methods. They found that Lewis acidic BF_3 reduced the Gibbs free energy of activation for the rate-determining step from 49.0 to 17.0 kcal/mol by facilitating proton transfer from the acetone−hydrogen peroxide adduct. No computational studies have considered metal-catalyzed Baeyer−Villiger reaction pathways.

Tin-containing redox molecular sieves clearly demonstrate great potential as industrial catalysts for accomplishing environmentally friendly Baeyer−Villiger oxidations with hydrogen peroxide. Improved understanding of their catalytic mechanism should assist future efforts at enhancing their performance. We have therefore undertaken a comprehensive computational study of reaction pathways for tin-catalyzed Baeyer−Villiger oxidation of the model ketone acetone with hydrogen peroxide.

Computational Methodology

All calculations reported here were performed with Gaussian98[41] and NBO version 5.0[42] software. Density functional theory as implemented in the restricted B3LYP hybrid exchange-correlation scheme was used to include some effects of electron correlation with only a marginal increase in computational cost over Hartree−Fock methods. All results have been obtained for cluster geometries optimized in the gas phase. Solvent continuum effects have been considered for selected cases using the gas-phase optimized geometries in conjunction with the integral equation formalism of the polarizable continuum model (IEF-PCM).[43] All stationary points have been characterized with a full vibrational analysis, and all reported energy differences include zero point energy corrections. Thermochemistry calculations have been performed at 298.15 K and 1 atm to account for entropy effects. The zero point energy corrections and thermochemistry results (ΔH, ΔS, and ΔG) have not been scaled. Tin was modeled by a LANL2DZ effective core potential with additional polarization (d-type) and diffuse (p-type) functions as developed by Check et al.[44] A 6-311+G(d,p) basis set was used for all other atoms. Natural bond orbital (NBO) methods were used to analyze the resultant wave functions in terms of optimally chosen, localized orbitals corresponding to a Lewis structure representation of chemical bonding.[45] The occupancies of natural bond orbitals are highly condensed in the most important one-center (lone pair) and two-center (bond) members, with electron delocalization effects, or donor−acceptor interactions, treated via standard perturbative techniques.

For most calculations, the tin active site was modeled with unconstrained clusters representing the first coordination sphere of the tin center. The simplicity of such a cluster model limits the absolute accuracy of the results reported here with regards to real tin-containing redox molecular sieve catalysts. Our computational methodology compromises on model rigor to permit an extremely wide survey of Baeyer−Villiger reaction pathways to be accomplished on a reasonable time scale. This

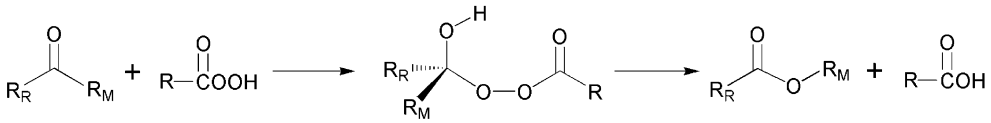

Figure 2. General two-step Criegee reaction mechanism for Baeyer−Villiger oxidation of ketones with peroxycarboxylic acid oxidants.

study seeks to elucidate important energetic trends that are relevant to the Sn(IV)−H_2O_2 catalytic system in general rather than to describe the absolute energetics applicable to any specific tin-based catalyst. Any systematic errors arising from the small cluster model should apply to all species and are expected to have a much smaller effect on calculated energy differences. The two chief sources of potential nonsystematic error for this model are the lack of steric constraints and the alterations in the electronic properties of the tin center and neighboring oxygen atoms caused by cluster truncation. These issues have been addressed for several of the trends reported here using constrained clusters representing the second coordination sphere of the tin active site for a typical molecular sieve support (see details below). Chemical accuracy may be approached by utilizing embedded cluster methods or constrained multiple coordination sphere cluster models to represent the extended environment of the tin active site. Such calculations will require substantially larger computational resources but could be justified to investigate how particular molecular sieve lattices influence the local tin environment and the general reactivity patterns described here.

The tin active site in the absence of ligands has been modeled with a $Sn(OH)_4$ cluster. This cluster was chosen on the basis of experimental characterization of the local tin environment in tin-containing redox molecular sieves performed by Corma and co-workers[25−27] and researchers at the National Chemical Laboratory in Pune, India.[46−51] Both groups have found that tin atoms isomorphously substitute for silicon atoms in the molecular sieve framework; the tin atoms are atomically isolated from one another and tetrahedrally coordinated under vacuum conditions. The hydroxyl groups in our single coordination sphere $Sn(OH)_4$ cluster model therefore may represent either bonds to framework silicon atoms (Sn−O−Si modeled as Sn−O−H) or hydrolyzed framework linkages. We focus our attention on proton-transfer reactions involving the participation of a single hydroxyl group and treat the other three hydroxyl groups as equivalent, nonreactive structural units. Water, hydrogen peroxide, and acetone molecules were added to the $Sn(OH)_4$ cluster as ligands on tin. Ligated clusters will be labeled as $Sn(OH)_4$−L, where L is the ligand. Transition states have been calculated for the formation of tin hydroperoxo species from various $Sn(OH)_4$ complexes possessing a single hydrogen peroxide ligand. The existence of a single negative vibrational mode was confirmed for each optimized transition-state structure, and intrinsic reaction coordinate (IRC) calculations were used to verify the reactants and products corresponding to that mode.[52] The resulting tin hydroperoxo intermediates have been modeled with $Sn(OH)_3(OOH)$ clusters.

Several potential reaction pathways for the Baeyer−Villiger oxidation of the model ketone acetone with hydrogen peroxide have been examined using the $Sn(OH)_4$ or $Sn(OH)_3(OOH)$ active site models. Preference is given to the use of the Gibbs free energy of activation over the electronic, or potential, energy of activation as a basis for comparing alternative reaction pathways. The rate constant (k) for an elementary reaction step is defined in terms of the Gibbs activation barrier (ΔG_A) as

$$k = \kappa(k_B T/h) \exp(-\Delta G_A/RT) = \kappa(k_B T/h) \exp(\Delta S_A/R) \exp(-\Delta H_A/RT) \quad (1)$$

where κ is the transmission coefficient, k_B is the Boltzmann constant, and ΔS_A and ΔH_A are the entropic and enthalpic activation barriers, respectively. By incorporation of entropy effects, the Gibbs activation barrier provides a more complete representation of intrinsic reaction kinetics at nonzero temperatures than the electronic activation barrier.

To assess utility of the minimal $Sn(OH)_4$ and $Sn(OH)_3(OOH)$ cluster calculations, the second coordination sphere of the tin active site has been added and modeled with a constrained $Sn(OSiH_3)_3(OH)$ cluster for selected cases. This cluster was constructed by substituting a tin atom for the T-3 silicon atom in the monoclinic MFI framework using the X-ray diffraction coordinates of van Koningsveld et al.[53] A portion of the MFI framework including the tin atom and its first three coordination spheres was then extracted from the crystal lattice, and hydrogen atoms were added to the dangling bonds of the terminal oxygen atoms along the original bonding direction with the adjacent silicon atoms to yield a $Sn[OSi(OH)_3]_4$ cluster. This cluster was then optimized with the hydrogen atom positions fixed. The first two coordination spheres of the optimized $Sn[OSi(OH)_3]_4$ cluster were then extracted, and hydrogen atoms were added to the dangling bonds of the terminal silicon atoms to yield a $Sn(OSiH_3)_4$ cluster. One siloxyl group on tin was replaced with a hydroxyl group, and the positions of the remaining silicon atoms were fixed in all subsequent optimizations. The resulting constrained $Sn(OSiH_3)_3(OH)$ cluster was used as the starting point for all calculations involving the second coordination sphere model.

Results and Discussion

Noncatalyzed Baeyer−Villiger Oxidation. It is generally agreed that in the absence of general or specific acid−base catalysis, the Baeyer−Villiger oxidation with peroxycarboxylic acids follows the two-step mechanism shown in Figure 2.[1−4] In the first step, the peracid adds across the carbonyl double bond to yield a tetrahedral perhemiketal species known as the "Criegee" intermediate. In the second step, the Criegee intermediate rearranges in a concerted manner to yield the ester product with a carboxylic acid as the leaving group. The second step is often the rate-determining step for the reaction. The noncatalyzed Baeyer−Villiger oxidation with hydrogen peroxide as oxidant is hypothesized to proceed in a similar manner except water is the leaving group. It is generally thought that the inactivity of hydrogen peroxide as a Baeyer−Villiger oxidant can be attributed to the poor leaving group properties (i.e., greater basicity) of water compared to carboxylic acids.

Alternative proposals for the general Baeyer−Villiger reaction mechanism proceed through dioxirane or carbonyl oxide intermediates.[3] Corma et al.[25,26] have shown conclusively with ^{18}O isotopic labeling experiments that such mechanisms are not operable for their tin-containing redox molecular sieve catalysts. We have therefore confined our mechanistic explorations to reaction pathways that proceed through Criegee-like intermediates.

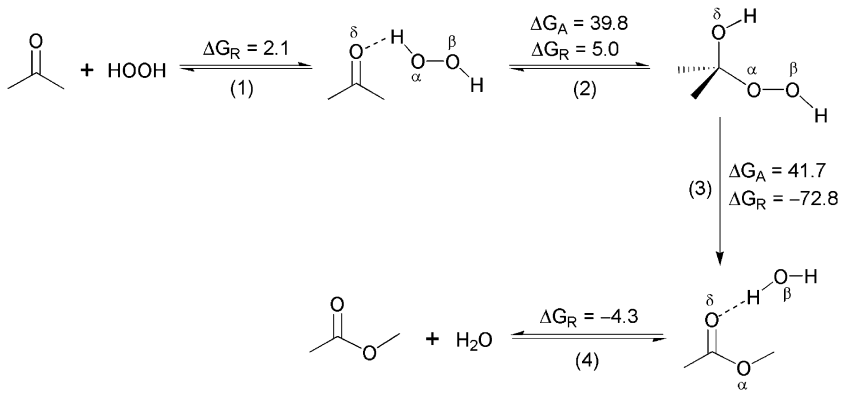

Figure 3. Mechanism I: the noncatalyzed Baeyer−Villiger oxidation of acetone with hydrogen peroxide. Gibbs free energies of reaction (ΔG_R) and activation (ΔG_A) are reported in kcal/mol, elementary steps are numbered in parentheses, and dashed lines represent hydrogen-bonding interactions.

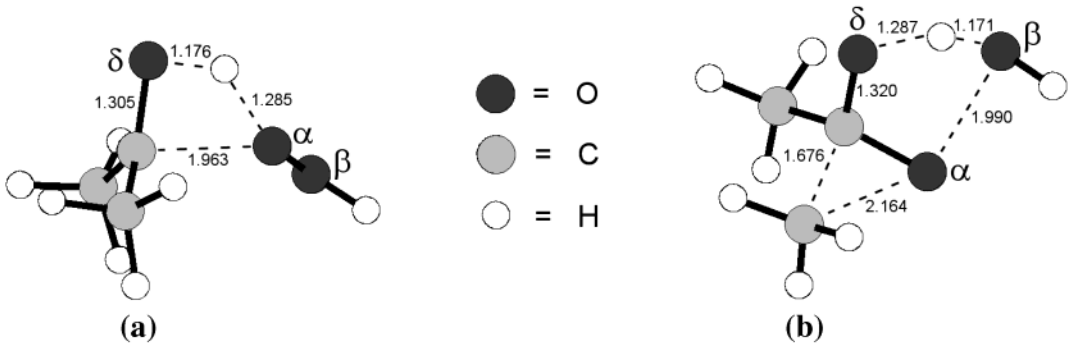

Figure 4. Optimized transition-state geometries for mechanism I: (a) Criegee intermediate formation (step 2); (b) Baeyer−Villiger rearrangement of the Criegee intermediate (step 3). Bonds in the process of breaking or forming are shown with dashed lines; bond distances are in Å.

The complete reaction mechanism for the noncatalyzed Baeyer−Villiger oxidation of acetone with hydrogen peroxide (mechanism I) is shown schematically in Figure 3 along with the calculated Gibbs free energies of reaction (ΔG_R) and activation (ΔG_A) for each elementary step. In the first step of mechanism I, hydrogen peroxide donates a hydrogen bond to the carbonyl oxygen Oδ. In step 2, hydrogen peroxide adds across the carbonyl double bond to generate the Criegee intermediate. The transition state for this step is shown in Figure 4a, and the activation barrier is 39.8 kcal/mol. NBO analysis of the transition-state wave function indicates that the addition of hydrogen peroxide to acetone proceeds through two principal donor−acceptor interactions: (1) a $n_{O\alpha} \rightarrow \pi_{C=O\delta}^*$ donation from a lone pair on the attacking hydrogen peroxide oxygen Oα to the π-type antibond orbital of the carbonyl group and (2) a $n_{O\delta} \rightarrow \sigma_{O\alpha-H}^*$ donation from a lone pair on the carbonyl oxygen Oδ to the $\sigma_{O\alpha-H}^*$ antibond orbital of the hydrogen peroxide oxidant (see Figure 3 for nomenclature). The first interaction breaks the carbonyl π-bond and creates a bond between the carbonyl carbon and the hydrogen peroxide oxygen Oα; the second interaction transfers the proton from Oα to Oδ. In step 3, the Criegee intermediate undergoes Baeyer−Villiger rearrangement to yield methyl acetate with the water leaving group hydrogen bonded to the carbonyl oxygen. This concerted reaction step is highly exothermic ($\Delta G_R = -72.8$ kcal/mol) and irreversible. The transition state for step 3 is shown in Figure 4b, and the activation barrier is 41.7 kcal/mol. The two main donor−acceptor interactions in the transition state for step 3 are (1) a $\sigma_{C-C} \rightarrow \sigma_{O\alpha-O\beta}^*$ donation from the bond between the original carbonyl carbon and the migrating carbon to the $\sigma_{O\alpha-O\beta}^*$ antibond orbital of the peroxo group and (2) a $n_{O\beta} \rightarrow \sigma_{O\delta-H}^*$ donation from a lone pair on the distal hydroperoxo oxygen Oβ to the $\sigma_{O\delta-H}^*$ antibond orbital. The first interaction results in methyl group migration and cleavage of the peroxo bond; the second interaction abstracts the proton from Oδ to produce the water leaving group and regenerate the carbonyl group of the ester. In the final step of mechanism I, the methyl acetate and water products separate.

The Gibbs activation barriers for Criegee intermediate formation (step 2) and Baeyer−Villiger rearrangement (step 3) are both very high at 39.8 and 41.7 kcal/mol, respectively. Carlqvist et al.[40] have studied the same Baeyer−Villiger mechanism, and they calculated similar activation barriers of 40.1 and 43.3 kcal/mol using a B3LYP/6-31+G(d) methodology. These high activation barriers are in accordance with the experimental observation that Baeyer−Villiger oxidation of ketones with hydrogen peroxide does not occur to any significant extent without catalytic activation.

Relative Stabilities of Tin Complexes and Activation of Hydrogen Peroxide. It is possible that the ketone substrate and the hydrogen peroxide oxidant may be activated for Baeyer−Villiger oxidation via coordination at tin. The relative stabilities of $Sn(OH)_4$ clusters bearing ketone and hydrogen peroxide ligands are summarized in Table 1. The addition of a single acetone, hydrogen peroxide, or water ligand to the tin center is electronically exothermic with $\Delta E = -10.6$, -13.6, or -10.9 kcal/mol, respectively. The entropy loss of binding these ligands increases the Gibbs free energy of the ligated clusters by about 11−13 kcal/mol at 298 K. As a result, the net Gibbs free energy change for the addition of a single acetone, hydrogen peroxide, or water ligand to $Sn(OH)_4$ is $\Delta G = +2.3$, -2.5, or -1.0 kcal/mol, respectively. Comparison of the results for acetone, methyl isopropyl ketone, and methyl *tert*-butyl ketone indicates that increased ketone branching augments the coordinative interaction between the carbonyl group and the tin center. The electronic energy change for addition of an acetone or water

TABLE 1: Relative Stabilities of Unconstrained $Sn(OH)_4$ and Constrained $Sn(OSiH_3)_3(OH)$ Complexes[a]

	thermochemistry at 298 K			
	ΔE	ΔH	$T\Delta S$	ΔG
$Sn(OH)_4$ Cluster				
$Sn(OH)_4$	0.0	0.0	0.0	0.0
$Sn(OH)_4-H_2O$	−10.9	−12.0	−11.0	−1.0
$Sn(OH)_4-H_2O_2$	−13.6	−14.2	−11.6	−2.5
$Sn(OH)_4-OC(CH_3)_2$	−10.6	−11.0	−13.2	2.3
$Sn(OH)_4-OC(CH_3)[CH(CH_3)_2]$	−12.3	−12.1	−11.9	−0.2
$Sn(OH)_4-OC(CH_3)[C(CH_3)_3]$	−14.5	−13.9	−11.0	−2.9
$Sn(OH)_4-(H_2O_2, H_2O)$	−19.4	−20.7	−21.5	0.8
$Sn(OH)_4-(H_2O_2, H_2O[HB])$	−24.5	−26.1	−21.9	−4.2
$Sn(OH)_4-(H_2O_2, OC(CH_3)_2)$	−19.2	−19.7	−23.4	3.7
$Sn(OSiH_3)_3(OH)$ Cluster				
$Sn(OSiH_3)_3(OH)$	0.0	0.0	0.0	0.0
$Sn(OSiH_3)_3(OH)-H_2O_2$	−9.3	−9.6	−13.6	4.1
$Sn(OSiH_3)_3(OH)-OC(CH_3)_2$	−7.3	−7.0	−13.5	6.5
$Sn(OSiH_3)_3(OH)-(H_2O_2, H_2O[HB])$	−19.1	−20.3	−24.1	3.8

[a] Energy changes in kcal/mol calculated relative to the nonligated $Sn(OH)_4$ or $Sn(OSiH_3)_3(OH)$ cluster and coordinating species at infinite separation.

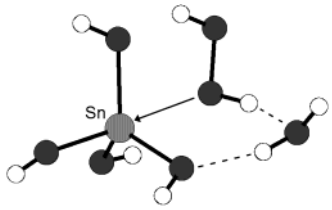

Figure 5. Optimized geometry for $Sn(OH)_4-(H_2O_2, H_2O[HB])$ in which a water molecule bridges the hydrogen peroxide ligand and a hydroxyl oxygen via dual hydrogen-bonding interactions. The arrow represents coordinative interaction with tin; dashed lines represent hydrogen-bonding interactions.

ligand to the $Sn(OH)_4-H_2O_2$ cluster is about −5.5 kcal/mol. The entropy loss for binding a second ligand to tin, however, is once again on the order of 10−12 kcal/mol, and as a result, the relative stabilities of the $Sn(OH)_4-(H_2O_2, H_2O)$ and $Sn(OH)_4-(H_2O_2, OC(CH_3)_2)$ clusters are less than the monoligated clusters.

We have also considered the case where a water molecule coordinates the $Sn(OH)_4-H_2O_2$ cluster by simultaneously donating a hydrogen bond to a hydroxyl oxygen atom and receiving a hydrogen bond from the protic hydrogen peroxide ligand. This cluster with a water molecule in such a hydrogen-bonded (HB) bridging position has been labeled $Sn(OH)_4-(H_2O_2, H_2O[HB])$; the optimized structure is provided in Figure 5. As shown in Table 1, the presence of the bridging water molecule confers about 11 kcal/mol of electronic stabilization to the $Sn(OH)_4-(H_2O_2, H_2O[HB])$ cluster. This electronic stabilization is almost completely offset by the entropy loss arising from the restricted motion of the water molecule participating in the two hydrogen bonds. The addition of the bridging water molecule therefore only slightly improves the relative stability of the $Sn(OH)_4$ complex. Similar results are obtained for the constrained $Sn(OSiH_3)_3(OH)-(H_2O_2, H_2O[HB])$ cluster (Table 1). Larger hydrogen-bonded networks involving multiple protic species are beyond the scope of the present study.

The addition of a hydrogen peroxide ligand to tin in the absence of steric constraints is 4.8 kcal/mol more exothermic than the addition of an acetone ligand. This difference is reduced to 2.4 kcal/mol when the tin active site is modeled with the constrained $Sn(OSiH_3)_3(OH)$ clusters. In either case, the results in Table 1 indicate that hydrogen peroxide competes favorably with acetone for coordination at the tin active site. The strength of carbonyl coordination is enhanced by increased ketone branching, so that larger ketone substrates, such as the ones employed in the experiments by Corma et al.,[25−27] might better compete with hydrogen peroxide. In an actual redox molecular sieve catalyst, however, the coordination strength of ketones larger than acetone may be significantly affected by steric or dispersion interactions between substituents on the carbonyl group and the molecular sieve framework. Furthermore, the relative intraporous concentrations of the ketone substrate and the hydrogen peroxide oxidant will be controlled by the molecular sieve pore properties. Hence, the cluster models used in this study are not useful for characterizing the competitive adsorption of large ketones and hydrogen peroxide for tin-containing redox molecular sieves.

We have studied the formation of tin hydroperoxo $Sn(OH)_3(OOH)$ species from the $Sn(OH)_4$ clusters in Table 1 possessing a hydrogen peroxide ligand. The calculated activation energies and reaction energies are summarized in Table 2. We considered two different mechanisms for tin hydroperoxo intermediate formation, depending upon the absence or presence of a water molecule in the hydrogen-bonded bridging position. For the $Sn(OH)_4-H_2O_2$ and $Sn(OH)_4-(H_2O_2, H_2O)$ clusters, the hydrogen peroxide ligand transfers a hydrogen from the oxygen coordinating the tin center to the nearest hydroxyl oxygen. This proton-transfer step results in the transformation of the coordinated hydrogen peroxide ligand into a hydroperoxo group on tin and the transformation of a hydroxyl group on tin into a coordinated water ligand. This reaction pathway is illustrated in Figure 6a for the $Sn(OH)_4-H_2O_2$ reactant cluster. In the case of $Sn(OH)_4-(H_2O_2, H_2O[HB])$, the hydrogen peroxide ligand transfers a hydrogen from the oxygen coordinating the tin center to the water molecule in the hydrogen-bonded bridging position, and the water molecule simultaneously transfers one of its hydrogens to a hydroxyl oxygen. These two proton-transfer steps occur in a concerted manner through the two pre-existing hydrogen bonds the bridging water molecule shares with the hydrogen peroxide ligand and the hydroxyl oxygen. This reaction pathway is illustrated in Figure 6b. The net result is the same as the previous case: the transfer of a hydrogen from the hydrogen peroxide ligand to a hydroxyl oxygen and the formation of a hydroperoxo group and water ligand on the titanium center. The product species has been labeled $Sn(OH)_3(OOH)-(H_2O, H_2O[HB-O\alpha])$; the bridging water molecule denoted by $H_2O[HB-O\alpha]$ simultaneously receives a hydrogen bond from the water ligand on tin and donates a hydrogen bond to the proximal oxygen $O\alpha$ of the hydroperoxo group.

The activation barriers for formation of the tin hydroperoxo species listed in Table 2 are similar to the activation barriers calculated for analogous titanium hydroperoxo species in our previous study.[54] Similar trends in reactivity are also observed as a result of water coordination at the metal active site. The octahedral $Sn(OH)_4-(H_2O_2, H_2O)$ cluster requires significantly less deformation than the pentahedral $Sn(OH)_4-H_2O_2$ cluster to accomplish proton transfer from the hydrogen peroxide ligand to the hydroxyl oxygen. The bridging water molecule in the $Sn(OH)_4-(H_2O_2, H_2O[HB])$ cluster dramatically facilitates proton transfer via the hydrogen bonds it shares with the hydrogen peroxide ligand and the hydroxyl group. As a result, the transition states for $Sn(OH)_4-(H_2O_2, H_2O)$ and $Sn(OH)_4-(H_2O_2, H_2O[HB])$ both occur earlier along the reaction coordinate than the transition state for $Sn(OH)_4-H_2O_2$, and their activation barriers are lower. A similar decrease in the activation

TABLE 2: Activation Barriers and Reaction Energies for the Formation of Tin Hydroperoxo Intermediates Possessing Various Coordination Environments (in kcal/mol)

	activation barrier		reaction energy	
intermediate formation reaction	ΔE_A	ΔG_A	ΔE_R	ΔG_R
$Sn(OH)_4-H_2O_2 \rightarrow Sn(OH)_3(OOH)-H_2O$	14.8	15.4	2.8	2.5
$Sn(OH)_4-(H_2O_2, H_2O) \rightarrow Sn(OH)_3(OOH)-2H_2O$	11.4	12.2	3.0	3.2
$Sn(OH)_4-(H_2O_2, H_2O[HB]) \rightarrow Sn(OH)_3(OOH)-(H_2O, H_2O[HB-O\alpha])$	7.6	8.7	2.6	2.5
$Sn(OSiH_3)_3(OH)-H_2O_2 \rightarrow Sn(OSiH_3)_3(OOH)-H_2O$	14.0	13.8	0.6	1.2
$Sn(OSiH_3)_3(OH)-(H_2O_2, H_2O[HB]) \rightarrow Sn(OSiH_3)_3(OOH)-(H_2O, H_2O[HB-O\alpha])$	7.5	8.7	1.6	1.7

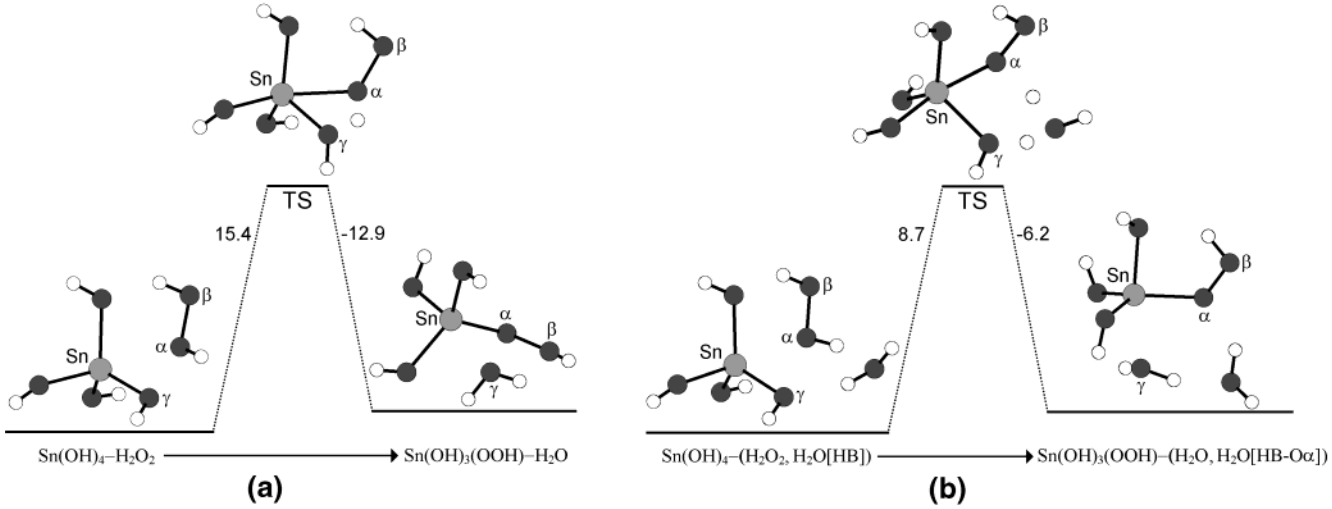

Figure 6. Reaction pathways for tin hydroperoxo intermediate formation in the (a) absence and (b) presence of the hydrogen-bonded bridging water molecule. Gibbs free energy changes are in kcal/mol.

TABLE 3: Relative Stabilities for Unconstrained $Sn(OH)_3(OOH)$ Complexes[a]

	thermochemistry at 298 K			
$Sn(OH)_3(OOH)$ cluster	ΔE	ΔH	$T\Delta S$	ΔG
$Sn(OH)_3(OOH)$	0.0	0.0	0.0	0.0
$Sn(OH)_3(OOH)-H_2O$	−9.7	−10.8	−10.9	0.2
$Sn(OH)_3(OOH)-H_2O$ (five-membered ring)	−11.3	−12.6	−11.5	−1.1
$Sn(OH)_3(OOH)-OC(CH_3)_2$	−10.7	−11.1	−13.4	2.3
$Sn(OH)_3(OOH)-OC(CH_3)[CH(CH_3)_2]$	−12.4	−12.2	−12.0	−0.2
$Sn(OH)_3(OOH)-OC(CH_3)[C(CH_3)_3]$	−14.6	−14.0	−11.2	−2.8
$Sn(OH)_3(OOH)-(H_2O, OC(CH_3)_2)$	−16.3	−17.6	−24.0	6.5
$Sn(OH)_3(OOH)-(H_2O, OC(CH_3)_2)$ (five-membered ring)	−17.6	−19.2	−25.1	5.9

[a] Energy changes in kcal/mol calculated relative to the nonligated $Sn(OH)_3(OOH)$ cluster and coordinating species at infinite separation.

barrier occurs when a bridging water molecule is added to the constrained $Sn(OSiH_3)_3(OH)-H_2O_2$ cluster (Table 2).

The activation barriers for hydrogen peroxide activation listed in Table 2 are all fairly low, especially compared to the rate-determining steps for the Baeyer−Villiger reaction mechanisms presented below. Tin hydroperoxo species will therefore likely exist under typical reaction conditions. It is generally accepted on the basis of extensive experimental and computational studies that similar titanium hydroperoxo species are the active intermediates in oxidation reactions with hydrogen peroxide catalyzed by titanium-containing redox molecular sieves. Researchers at the National Chemical Laboratory in Pune, India, have shown that tin-containing redox molecular sieves activate hydrogen peroxide for the hydroxylation of aromatic compounds[49,55−57] and activate *tert*-butyl hydroperoxide for the epoxidation of alkenes,[46] but they have not examined the nature of the active intermediates.

The relative stabilities of several tin hydroperoxo complexes are listed in Table 3. The hydroperoxo moiety in the $Sn(OH)_3$-(OOH) complex invariably possesses monodentate coordination to the tin center. This result contrasts with results obtained previously for $Ti(OH)_3(OOH)$ complexes, where both bidentate and monodentate coordination are possible.[54] Protic ligands on

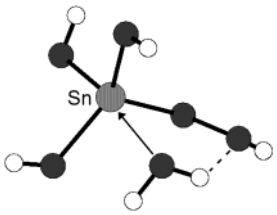

Figure 7. Optimized geometry for the $Sn(OH)_3(OOH)-H_2O$ cluster in which the water ligand donates a hydrogen bond to the distal hydroperoxo oxygen via a five-membered ring. The arrow represents coordinative interaction with tin; the dashed line represents hydrogen-bonding interaction.

tin may donate a hydrogen bond to the distal oxygen of the hydroperoxo group and thereby form a five-membered ring intermediate, as shown for $Sn(OH)_3(OOH)-H_2O$ in Figure 7. Hydrogen bonding in a five-membered ring provides little additional stabilization to the tin hydroperoxo cluster (Table 3). The relative stabilities of the $Sn(OH)_3(OOH)$ clusters follow trends similar to the ones described for the $Sn(OH)_4$ clusters above.

NBO analysis reveals that the primary donor−acceptor interactions stabilizing ligand coordination at the $Sn(OH)_4$ or

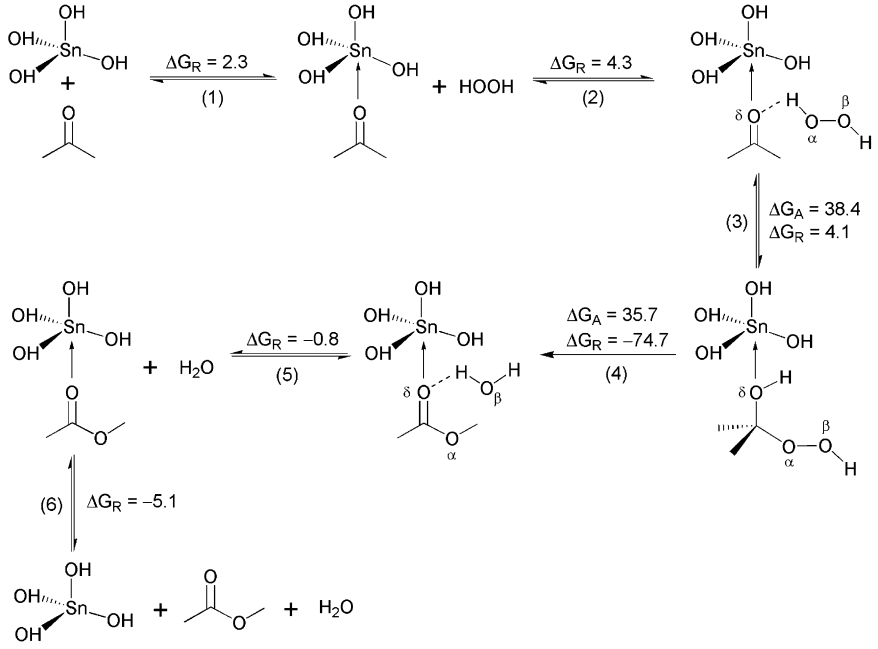

Figure 8. Mechanism II: tin-catalyzed Baeyer−Villiger oxidation of acetone with hydrogen peroxide. Acetone is coordinated to $Sn(OH)_4$ and reacts directly with free hydrogen peroxide. The structural arrows represent coordinative interactions with tin; dashed lines represent hydrogen-bonding interactions.

$Sn(OH)_3(OOH)$ clusters are donations from the lone pair on the ligand oxygen to the four σ_{Sn-O}* antibond orbitals of the central SnO_4 tetrahedron. Second-order perturbation theory estimates of the stabilization energy accompanying these hypervalent donor−acceptor interactions range between 3 and 14 kcal/mol, depending upon the ligand identity and the orientation of its lone pair orbitals with respect to the four σ_{Sn-O}* antibond orbitals. This result can be contrasted with monoligated $Ti(OH)_4$ and $Ti(OH)_3(OOH)$ clusters, which demonstrate a single prominent donor−acceptor interaction with a strength of 35−55 kcal/mol between the ligand lone pair orbital and the σ_{Ti-O}* antibond orbital positioned trans to the ligand.[54] These differences in coordination behavior can be attributed to the open d-shell and sd^5 hybridization of titanium compared to the closed d-shell and sp^3 hybridization of tin.

$Sn(OH)_4$ as Lewis Acid Catalyst: Mechanism II. There are several potential reaction pathways for the Baeyer−Villiger oxidation of the model ketone acetone with hydrogen peroxide using the $Sn(OH)_4$ and $Sn(OH)_3(OOH)$ active site models. We first examined a tin-catalyzed Baeyer−Villiger reaction mechanism similar to that proposed by Corma et al.[25] They suggested that coordination of the ketone substrate at the Lewis acidic tin site activates the carbonyl group for reaction with free hydrogen peroxide. This reaction mechanism is shown in Figure 8 for the Baeyer−Villiger oxidation of acetone with hydrogen peroxide and will be referred to as mechanism II. Mechanism II is exactly analogous to the noncatalyzed mechanism I, the only difference being the coordination of the ketone substrate and Criegee intermediate to the tin active site. In the first two steps, acetone coordinates the tin center, and hydrogen peroxide donates a hydrogen bond to the carbonyl oxygen. In step 3, hydrogen peroxide adds across the carbonyl double bond to yield the Criegee intermediate coordinated to the tin site. The Criegee intermediate undergoes concerted Baeyer−Villiger rearrangement in step 4 to yield methyl acetate coordinated to the tin site with the water leaving group hydrogen bonded to the carbonyl oxygen. The transition states for steps 3 and 4 are shown in Figure 9a,b, respectively. In steps 5 and 6, the water and ester products desorb from the tin site.

It is apparent from the calculated energetics for mechanism II that coordination of acetone to tin does not significantly lower the activation barrier for formation of the Criegee intermediate. The activation barrier is 38.4 kcal/mol for mechanism II compared to 39.8 kcal/mol for the noncatalyzed mechanism I. NBO analysis helps elucidate the cause of this surprising reactivity trend. The addition reaction between free hydrogen peroxide and coordinated acetone in step 3 of mechanism II involves the same $n_{O\alpha} \rightarrow \pi_{C=O\delta}$* and $n_{O\delta} \rightarrow \sigma_{O\alpha-H}$* donor−acceptor interactions as step 2 of mechanism I. NBO analysis indicates that coordination of the carbonyl group on the tin active site stabilizes the $\pi_{C=O\delta}$* antibond and thereby promotes nucleophilic attack of Oα at the carbonyl carbon. The energy of the $\pi_{C=O\delta}$* antibond in acetone is 0.0164 Hartree when isolated and −0.0325 Hartree when coordinated to $Sn(OH)_4$ (1 Hartree = 627.5 kcal/mol). The enhanced electrophilicity of the $\pi_{C=O\delta}$* antibond is reflected in the transition-state geometry for step 3 (Figure 9a) by a greater carbonyl bond length and a shorter distance between the attacking hydrogen peroxide oxygen Oα and the carbonyl carbon compared to the corresponding transition state for mechanism I (Figure 4a). Coordination of the carbonyl group to tin also stabilizes the lone pairs on the carbonyl oxygen, and this interaction inhibits the carbonyl oxygen from abstracting the proton from hydrogen peroxide. The energy of the attacking lone pair on Oδ is −0.2700 Hartree when isolated and −0.4479 Hartree when coordinated to $Sn(OH)_4$. The reduced nucleophilicity of the carbonyl lone pair is reflected by the greater proximity of the transferring proton to the hydrogen peroxide oxygen Oα in the transition state for mechanism II compared to the transition state for mechanism I. Thus, the coordination of acetone to tin has two competing effects on the activation barrier for Criegee intermediate formation, and the end result is little change in that barrier relative to the noncatalyzed mechanism.

Coordination of the Criegee intermediate to $Sn(OH)_4$ reduces the activation barrier for Baeyer−Villiger rearrangement by 6.0

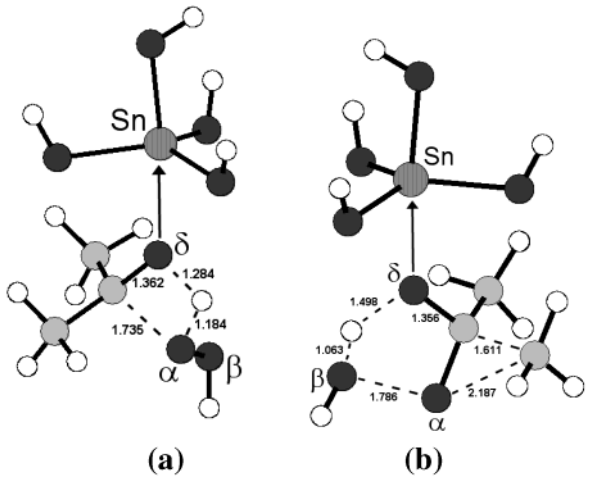

Figure 9. Optimized transition-state geometries for mechanism II: (a) Criegee intermediate formation (step 3); (b) Baeyer−Villiger rearrangement of the Criegee intermediate (step 4). Bonds in the process of breaking or forming are shown with dashed lines; bond distances are in Å.

kcal/mol compared to the noncatalyzed mechanism. The activation barrier for step 4 is lowered because the tin active site stabilizes the transition state more than the reactant. This increased stabilization is evidenced in the greater proximity of Oδ to tin in the transition-state cluster (Oδ−Sn = 2.132 Å) versus the reactant cluster (Oδ−Sn = 2.258 Å). The $n_{O\delta} \rightarrow \sigma_{Sn-O}^*$ donor−acceptor interactions characterizing the coordinative interaction between Oδ and tin are also significantly greater for the transition-state cluster.

The rate-determining step for mechanism II is formation of the Criegee intermediate (step 3), and it proceeds with an activation barrier near 40 kcal/mol. It is therefore unlikely that tin-containing redox molecular sieves catalyze the Baeyer−Villiger reaction through such a mechanism.

$Sn(OH)_4$ as Lewis Acid Catalyst: Mechanism III. An alternative mechanism in which the tin active site directly participates in the addition reaction between hydrogen peroxide and acetone is shown schematically in Figure 10 and will be referred to as mechanism III. In the first two steps, acetone coordinates the tin center, and hydrogen peroxide donates a hydrogen bond to one of the hydroxyl groups on tin. In step 3, the hydrogen peroxide oxygen Oα nucleophilically attacks the carbonyl carbon while the hydroxyl oxygen Oγ simultaneously abstracts the hydrogen-bonded proton from hydrogen peroxide. Similar to mechanisms I and II, attack of the carbonyl carbon proceeds through a $n_{O\alpha} \rightarrow \pi_{C=O\delta}^*$ donor−acceptor interaction. As a result of this interaction, the carbonyl π-bond is broken, and the carbonyl oxygen Oδ forms a bond with tin. The proton-transfer reaction between Oα and Oγ transforms the hydroxyl group on tin into a water ligand. Step 3 is a concerted reaction step and proceeds with an activation barrier of 11.1 kcal/mol; the transition state is shown in Figure 11a. The net result is the formation of the "chelated" Criegee intermediate $Sn(OH)_3[OC(OOH)(CH_3)_2]-H_2O$ shown in Figure 12a. In this species, the distal hydroperoxo oxygen Oβ coordinates the tin center through multiple $n_{O\beta} \rightarrow \sigma_{Sn-O}^*$ donor−acceptor interactions in the same manner described for solvent ligands earlier. Loss of the water ligand from the $Sn(OH)_3[OC(OOH)(CH_3)_2]-H_2O$ Criegee intermediate is exothermic by −4.3 kcal/mol (step 4); the structure of the nonligated $Sn(OH)_3[OC(OOH)(CH_3)_2]$ chelated Criegee intermediate is shown in Figure 12b. The chelated Criegee intermediates $Sn(OH)_3[OC(OOH)(CH_3)_2]-H_2O$ and $Sn(OH)_3[OC(OOH)(CH_3)_2]$ will be abbreviated as C-1 and C-2, respectively. Strukul and co-workers[16,17] and Katsuki and co-workers[21,22] have proposed the existence of similar chelated Criegee adducts as active intermediates for Baeyer−Villiger oxidations with hydrogen peroxide using homogeneous Pt^{II}(diphosphine) complexes and Zr^{IV}(salen) and Co^{III}(salen) complexes, respectively.

Intermediates C-1 (step 5) and C-2 (step 6) concertedly and irreversibly rearrange to produce methyl acetate bound to the tin center. In these rearrangement steps, the peroxo bond Oα−Oβ heterolytically cleaves to permit transfer of the proximal oxygen Oα to the migrating methyl group and transfer of the distal oxygen Oβ to the tin center. The Sn−Oδ bond simultaneously breaks, and the carbonyl group re-forms. The net result is regeneration of the $Sn(OH)_4$ active site and formation of the methyl acetate product coordinated to the tin center. The activation barriers for the Baeyer−Villiger rearrangement of intermediates C-1 and C-2 are 21.4 and 24.1 kcal/mol, respectively; the transition states are shown in Figure 11b,c. In the final steps of mechanism III, the water and methyl acetate products desorb from the tin active site.

The activation barriers for formation and Baeyer−Villiger rearrangement of the chelated Criegee intermediates C-1 and C-2 for mechanism III are much lower than the corresponding activation barriers for mechanisms I and II. NBO analysis again helps provide an explanation for the observed reactivity trends. The addition reaction between hydrogen peroxide and acetone in step 3 of mechanism III once again involves two principal donor−acceptor interactions: (1) a $n_{O\alpha} \rightarrow \pi_{C=O\delta}^*$ donation from a lone pair on the attacking hydrogen peroxide oxygen Oα to the π-type antibond orbital of the carbonyl group and (2) a $n_{O\gamma} \rightarrow \sigma_{O\alpha-H}^*$ donation from a lone pair on the hydroxyl group to the $\sigma_{O\alpha-H}^*$ antibond orbital of the hydrogen peroxide oxidant. Similar to mechanism II, coordination of the carbonyl group on the tin active site stabilizes the $\pi_{C=O\delta}^*$ antibond, thereby promoting nucleophilic attack of the carbonyl carbon. The primary difference between mechanisms II and III is that the proton is abstracted from hydrogen peroxide by a hydroxyl oxygen in mechanism III as opposed to the carbonyl oxygen in mechanism II. As a result, the stabilization of the carbonyl lone pairs via coordination to the electronegative tin center does not inhibit proton abstraction from hydrogen peroxide during step 3 of mechanism III. Furthermore, the addition of hydrogen peroxide to acetone in mechanism III occurs via a six-membered ring transition state (Figure 11a), which is much less strained than the four-membered ring transition states for mechanisms I and II (Figures 4a and 9a, respectively). The energy of the transition state is also significantly reduced by the ability of tin to strongly coordinate both Oδ and Oγ; the Sn−Oδ and Sn−Oγ bond distances are similar in the transition state.

The Baeyer−Villiger rearrangement of the chelated Criegee intermediates C-1 and C-2 is facilitated by the coordinative interaction between the distal hydroperoxo oxygen Oβ and the tin center. NBO analysis indicates that the $\sigma_{O\alpha-O\beta}^*$ antibond orbital in the Baeyer−Villiger transition state is polarized toward the proximal hydroperoxo oxygen Oα to promote the $\sigma_{C-C} \rightarrow \sigma_{O\alpha-O\beta}^*$ donor−acceptor interaction with the migrating carbon. The $\sigma_{O\alpha-O\beta}$ bond orbital is concomitantly polarized toward the distal hydroperoxo oxygen Oβ, and as a result, Oβ gains substantial negative charge in the transition state as shown in Table 4. The highly electronegative and positively charged tin atom stabilizes the developing negative charge on the distal hydroperoxo oxygen Oβ in the transition state. This electrostatic stabilization reduces the energy of the transition state for Baeyer−Villiger rearrangement of the chelated Criegee inter-

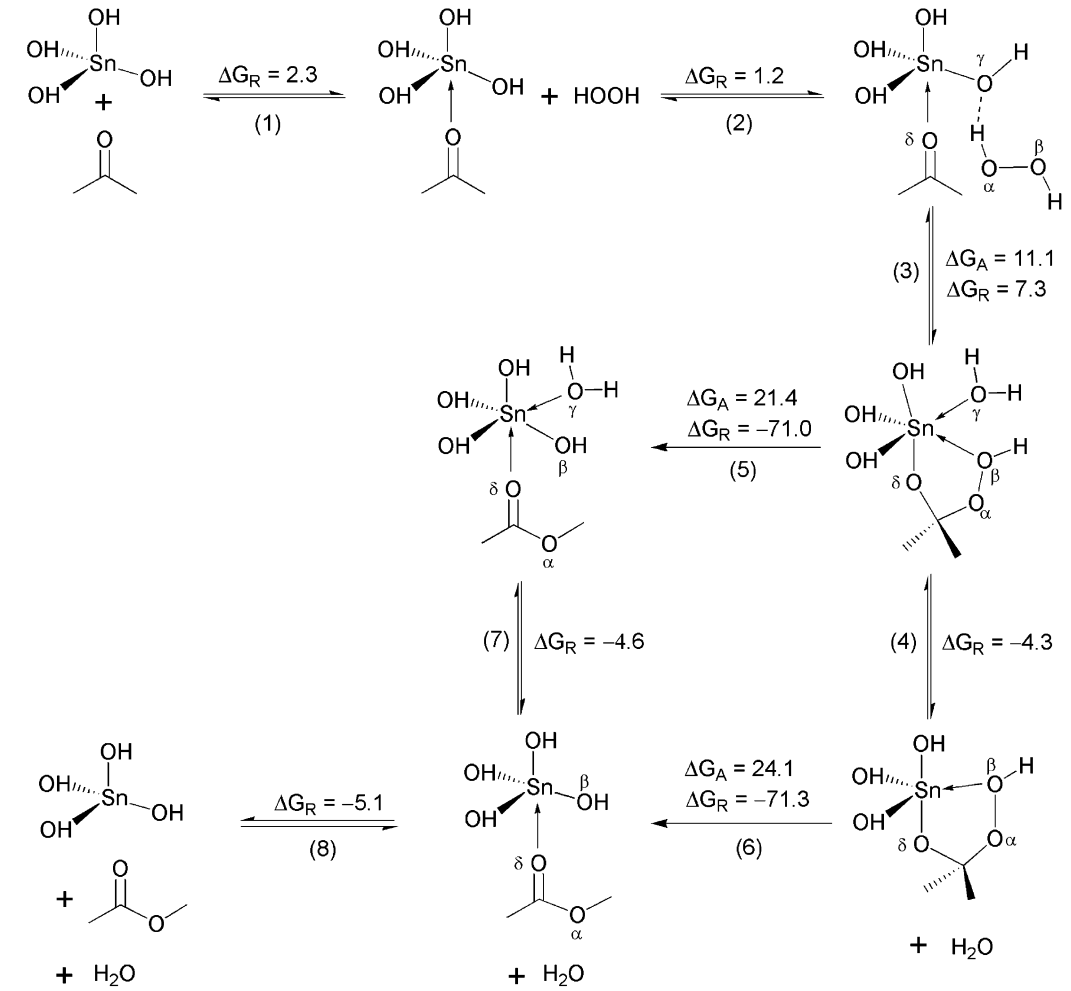

Figure 10. Mechanism III: tin-catalyzed Baeyer−Villiger oxidation of acetone with hydrogen peroxide. Hydrogen peroxide attacks the carbonyl carbon in acetone and simultaneously transfers a proton to a hydroxyl group oxygen in $Sn(OH)_4$ to form a chelated Criegee intermediate. The structural arrows represent coordinative interactions with tin; dashed lines represent hydrogen-bonding interactions.

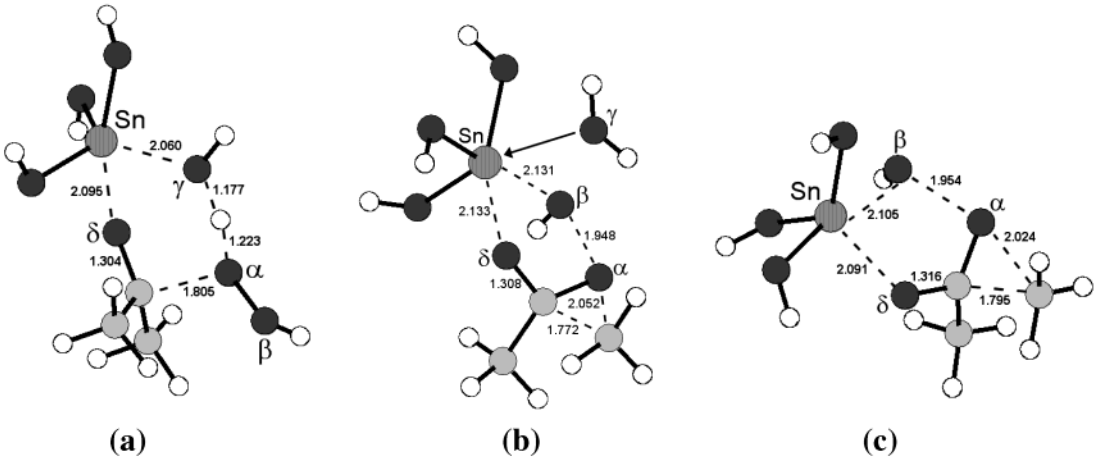

Figure 11. Optimized transition-state geometries for mechanism III: (a) formation of chelated Criegee intermediate C-1 (step 3); (b) Baeyer−Villiger rearrangement of intermediate C-1 (step 5); (c) Baeyer−Villiger rearrangement of intermediate C-2 (step 6). Bonds in the process of breaking or forming are shown with dashed lines; bond distances are in Å.

mediates relative to the nonchelated intermediates and thereby reduces the calculated activation barrier. In mechanisms I and II, water is the leaving group for heterolytic cleavage of the peroxo bond Oα–Oβ; in mechanism III, however, the leaving group is essentially SnOH.

The activation barriers for the irreversible rearrangement of intermediates C-1 (step 5) and C-2 (step 6) are much greater than the activation barrier for their formation (step 3) and therefore will control the overall Baeyer−Villiger reaction rate for mechanism III. The overall rate constant ($k_{overall}$) for a reaction pathway with an irreversible rate-determining step can be accurately approximated as

$$k_{overall} = \kappa(k_B T/h) \exp(-\Delta G_{total}/RT) \qquad (2)$$

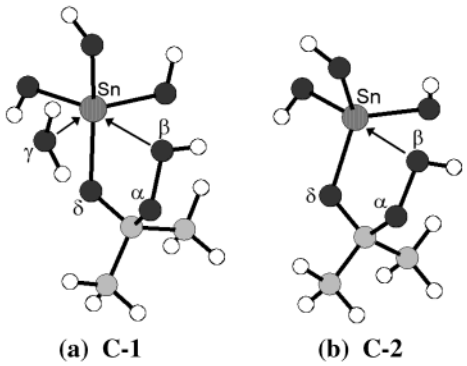

(a) C-1 (b) C-2

Figure 12. Optimized geometries of the chelated Criegee intermediates: (a) $Sn(OH)_3[OC(OOH)(CH_3)_2]-H_2O$ or C-1; (b) $Sn(OH)_3[OC(OOH)(CH_3)_2]$ or C-2.

TABLE 4: Atomic Charges in the Transition-State Clusters for Baeyer−Villiger Rearrangement of the Criegee Intermediate via Mechanisms I, II, and III

			atomic charge[a]		
mechanism	elementary step	ΔG_A[b]	Oα	Oβ	Sn/H[c]
I	3	41.7	−0.358	−0.706	0.484
II	4	35.7	−0.279	−0.583	0.527
III	5	21.4	−0.368	−0.887	2.739
III	6	24.1	−0.340	−0.884	2.731

[a] Atomic charges determined using natural population analysis. [b] Activation barrier in kcal/mol. [c] Charge on the atom (Sn or H) that bonds to the distal oxygen Oβ to form the leaving group when the peroxo bond is cleaved.

where the transmission coefficient κ is of order one and ΔG_{total} is the sum of the Gibbs activation barrier for the rate-determining step and the Gibbs free energy changes of reaction for all the preceding quasi-equilibrated steps. Mechanism III includes two possible reaction pathways for the overall reaction:

$$OC(CH_3)_2 + H_2O_2 \xrightarrow{Sn(OH)_4} OC(CH_3)(OCH_3) + H_2O \quad (3)$$

The reaction pathway for intermediate C-1 proceeds through steps 1−3 and 5 with $\Delta G_{total} = 32.2$ kcal/mol, whereas the reaction pathway for intermediate C-2 proceeds through steps 1−4 and 6 with $\Delta G_{total} = 30.6$ kcal/mol. The difference in ΔG_{total} for these two reaction pathways is within the margins of error for our calculations. Hence, our results indicate that both pathways will make significant contributions to the observed Baeyer−Villiger reaction rate.

In an actual redox molecular sieve catalyst, the tin center is isomorphously linked to the siliceous framework through Sn−O−Si bonds. The absolute energetics reported for mechanism III clearly only apply to the case where one of the Sn−O−Si framework linkages has been hydrolyzed and the resulting hydroxyl group participates in the proton-transfer reaction with hydrogen peroxide. Proton transfer from hydrogen peroxide to the oxygen in an intact Sn−O−Si framework linkage will yield a silanol group coordinating the tin center rather than a water ligand. It is expected that Baeyer−Villiger rearrangement of the chelated Criegee intermediate will remain the rate-determining step in this case. To investigate this hypothesis, we have calculated the activation barriers for variants of steps 3 and 5 using an $Sn(OH)_3(OSiH_3)$ active site model. The activation barrier for the variant of step 3 in which hydrogen peroxide transfers a proton to the siloxyl oxygen in $Sn(OH)_3(OSiH_3)-OC(CH_3)_2$ is 10.6 kcal/mol. Thus, proton transfer occurs just as readily with a siloxyl oxygen as with a hydroxyl oxygen. The presence of a silanol ligand (H_3SiOH) rather than a water ligand on the chelated Criegee intermediate $Sn(OH)_3[OC(OOH)(CH_3)_2]$ raises the activation barrier for Baeyer−Villiger rearrangement in step 5 from 21.4 to 23.5 kcal/mol.

$Sn(OH)_3(OOH)$ as Lewis Acid Catalyst: Mechanism IV. We have investigated two different mechanisms for Baeyer−Villiger oxidation of acetone with the tin hydroperoxo intermediate $Sn(OH)_3(OOH)$. We first considered a mechanism in which acetone adsorbs on the tin site and the hydroperoxo moiety attacks the carbonyl carbon. This mechanism is shown in Figure 13 for $Sn(OH)_3(OOH)$ clusters with and without a single water ligand and will be referred to as mechanism IV. Strukul and co-workers[17] have proposed a similar Baeyer−Villiger mechanism for their homogeneous Pt^{II}(diphosphine) catalysts. Step 1 is the overall reaction for the activation of hydrogen peroxide on the $Sn(OH)_4$ cluster to produce the tin hydroperoxo intermediate; this reaction proceeds in accordance with the mechanism described earlier. Steps 2−5 of mechanism IV describe the coordination of water and acetone at the tin center of the $Sn(OH)_3(OOH)$ cluster. In steps 6 and 7, the hydroperoxo group attacks the carbonyl carbon to yield the same chelated Criegee intermediates, C-1 and C-2, obtained in mechanism III. The transition states for steps 6 and 7 are shown in Figure 14a,b, respectively. A lone pair on the proximal hydroperoxo oxygen Oα donates electrons to the $\pi_{C=O\delta}$* antibond orbital of the carbonyl group. As a result, the carbonyl π-bond heterolytically cleaves, and the carbonyl oxygen Oδ forms a bond with tin. The activation barriers for formation of intermediates C-1 (step 7) and C-2 (step 6) are 11.0 and 13.7 kcal/mol, respectively. The octahedral $Sn(OH)_3(OOH)-(OC(CH_3)_2, H_2O)$ cluster requires less deformation to accomplish oxygen transfer from the hydroperoxo moiety to the carbonyl carbon than the pentahedral $Sn(OH)_3(OOH)-OC(CH_3)_2$ cluster. As a result, the relative energy of the transition state for chelated Criegee intermediate formation, and hence the activation barrier, is reduced when a water ligand coordinates the tin center. The activation barrier for the formation of intermediate C-1 in mechanism IV (step 7, 11.0 kcal/mol) is very similar to the corresponding barrier in mechanism III (step 3, 11.1 kcal/mol). The activation barrier for Criegee intermediate formation is once again much lower for mechanism IV compared to mechanisms I and II. The tin site stabilizes the $\pi_{C=O\delta}$* bond and thereby promotes nucleophilic attack by the hydroperoxo oxygen Oα. The addition reaction occurs via a four-membered ring transition state (Figure 14a) as it does in mechanisms I and II, but the four-membered ring in mechanism IV is not as strained due to the longer Sn−O bonds (compare with Figures 4a and 9a).

The chelated Criegee intermediates rearrange to form the product ester following the same energetic pathways as described for mechanism III (steps 9−12). The activation barriers for the Baeyer−Villiger rearrangement of intermediates C-1 and C-2 are once again 21.4 and 24.1 kcal/mol, respectively. These activation barriers are much greater than the activation barriers for the Criegee intermediate formation steps 6 and 7. Thus, Baeyer−Villiger rearrangement is also the rate-determining step for mechanism IV. Assuming quasi-equilibration of all preceding steps, the overall reaction kinetics will be the same as those for mechanism III. Hence, mechanism III and mechanism IV are kinetically indistinguishable from one another, and other tests will be required to determine if either or both are operable.

$Sn(OH)_3(OOH)$ as Peracid: Mechanism V. The second mechanism we considered involving the tin hydroperoxo intermediate is shown in Figure 15 and will be referred to as mechanism V. In this mechanism, the tin hydroperoxo species

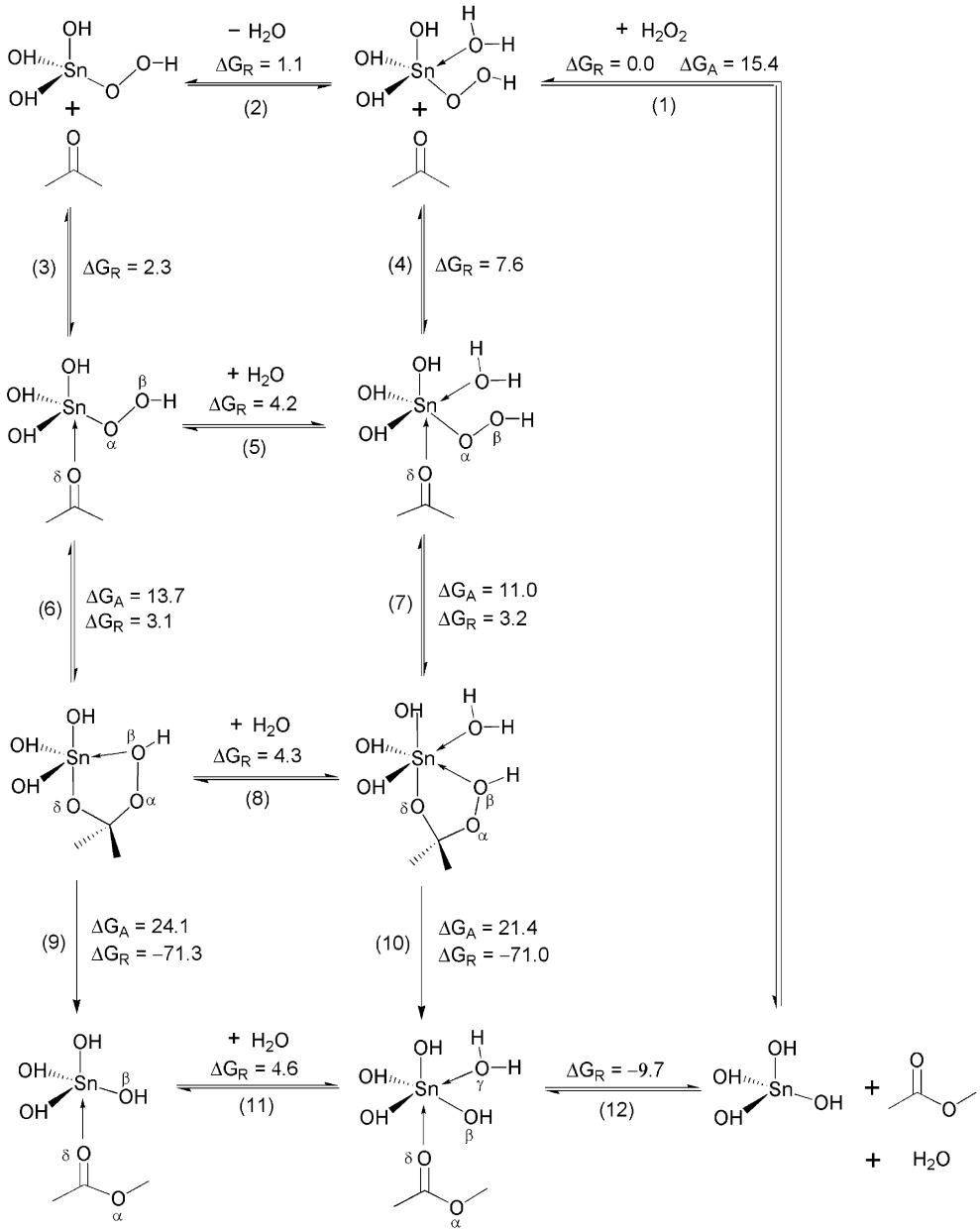

Figure 13. Mechanism IV: tin-catalyzed Baeyer−Villiger oxidation of acetone with hydrogen peroxide. Acetone is coordinated to $Sn(OH)_3(OOH)$ and reacts with the tin hydroperoxo group. Structural arrows represent coordinative interactions with tin; dashed lines represent hydrogen-bonding interactions.

behaves like a peracid. Step 1 of mechanism V is the overall reaction for the activation of hydrogen peroxide on the $Sn(OH)_4$ cluster to produce the tin hydroperoxo intermediate; this reaction proceeds in accordance with the mechanism described earlier. In step 2, the hydroperoxo moiety in $Sn(OH)_3(OOH)$ donates a hydrogen bond to the carbonyl oxygen of acetone. In step 3, the hydroperoxo group adds across the carbonyl double bond. The carbonyl oxygen Oδ abstracts the proton from the distal hydroperoxo oxygen Oβ via a $n_{O\delta} \rightarrow \sigma_{O\beta-H}^*$ donor−acceptor interaction while the proximal hydroperoxo oxygen Oα simultaneously attacks the carbonyl carbon via a $n_{O\alpha} \rightarrow \pi_{C=O\delta}^*$ interaction. During this addition reaction, the Sn−Oα bond breaks, and a new Sn−Oβ bond forms. The transition state for step 3 is shown in Figure 16a; the activation barrier is 24.1 kcal/mol. This activation barrier is substantially lower than the peroxide addition barriers for mechanisms I and II because the peroxide addition step in mechanism V occurs through a five-membered ring instead of a strained four-membered ring and the electronegative tin center is able to coordinate and stabilize both hydroperoxo oxygens Oα and Oβ in the transition state.

The end result of step 3 is the formation of a new chelated Criegee intermediate $Sn(OH)_3[OOC(OH)(CH_3)_2]$ shown in Figure 17; this intermediate will be referred to as C-3. Intermediate C-3 differs from intermediates C-1 and C-2 (Figure 12a,b)) by having a formal bond between tin and the peroxo group and a coordinative interaction between tin and the original carbonyl oxygen Oδ. Intermediate C-3 may rearrange concertedly via step 4 to produce methyl acetate. The migrating methyl group attacks the peroxo oxygen Oα while a lone pair on the distal oxygen Oβ abstracts the proton from Oδ. As a result, the Oα−Oβ bond is broken, and the $Sn(OH)_4$ active site is regenerated. This rearrangement step has a very high activation barrier of 44.8 kcal/mol and probably does not occur to any significant extent.

Intermediate C-3 can also rearrange via step 5 to form intermediate C-2. Proton donation from Oδ to Oβ leads to the

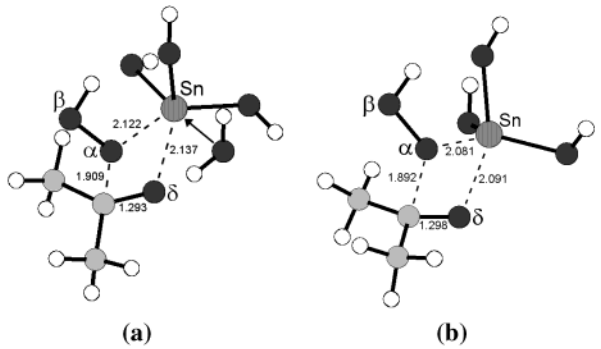

Figure 14. Optimized transition-state geometries for mechanism IV: (a) formation of chelated Criegee intermediate C-1 (step 7); (b) formation of chelated Criegee intermediate C-2 (step 6). Bonds in the process of breaking or forming are shown with dashed lines; bond distances are in Å.

formation of a new bond between tin and Oδ and the cleavage of the bond between tin and Oβ. The activation barrier for this transformation is 30.8 kcal/mol, and the transition state is shown in Figure 16b. The resulting intermediate C-2 undergoes Baeyer−Villiger rearrangement through step 6 in accordance with the previous mechanistic proposals. Comparison of the activation barrier for step 4 with the activation barriers for steps 5 and 6 indicates that mechanism V will proceed through steps 1−3, 5, 6, and 8. The rate-determining step for this reaction pathway is step 5, the rearrangement of intermediate C-3 to intermediate C-2. The overall rate constant for the Baeyer−Villiger reaction via mechanism V can be approximated once again using eq 2 with $\Delta G_{\text{total}} = 36.5$ kcal/mol. The corresponding reaction pathways for intermediate C-2 in mechanisms III and IV proceed with $\Delta G_{\text{total}} = 30.6$ kcal/mol. Thus, it is unlikely that tin catalyzes the Baeyer−Villiger reaction with hydrogen peroxide through mechanism V.

Constrained Cluster Calculations. Activation barriers have been calculated for the Baeyer−Villiger rearrangement of constrained cluster models representing the second coordination sphere of the chelated Criegee intermediates C-1 and C-2. The activation barriers for unconstrained $Sn(OH)_3[OC(OOH)(CH_3)_2]-H_2O$ (C-1) and constrained $Sn(OSiH_3)_3[OC(OOH)(CH_3)_2]-H_2O$ are very similar at 21.4 and 20.9 kcal/mol, respectively. The activation barrier for nonligated $Sn(OSiH_3)_3[OC(OOH)(CH_3)_2]$ is 26.3 kcal/mol, approximately 2 kcal/mol greater than the barrier for $Sn(OH)_3[OC(OOH)(CH_3)_2]$ (C-2). These results suggest that the degree to which a water ligand will reduce the rearrangement activation barrier in a real $Sn(IV)-H_2O_2$ catalytic oxidation system can depend on the local flexibility of the tin active site.

To investigate the effect of model description on overall reaction kinetics, we have also calculated activation barriers for formation of the chelated Criegee intermediate via mechanisms IV and V using the constrained $Sn(OSiH_3)_3(OOH)$ active site model. In step 3 of mechanism IV, the activation barrier for $Sn(OSiH_3)_3(OOH)$ is reduced approximately 5 kcal/mol relative to $Sn(OH)_3(OOH)$ primarily because acetone coordination in the reactant cluster is much less stable for the larger, rigidly constrained model. The decrease in the activation barrier for chelated Criegee intermediate formation using the constrained cluster model is kinetically insignificant, however, because the rate-determining step for mechanism IV remains the Baeyer−Villiger rearrangement. The value of ΔG_{total} for the overall reaction pathway proceeding through $Sn(OSiH_3)_3[OC(OOH)(CH_3)_2]$ is 34.3 kcal/mol compared to $\Delta G_{\text{total}} = 30.6$ kcal/mol for intermediate C-2.

In step 3 of mechanism V, the activation barrier changes negligibly from 24.1 to 24.2 kcal/mol as a result of using the constrained $Sn(OSiH_3)_3(OOH)$ cluster model. The activation barrier for intramolecular proton transfer in step 5 is slightly reduced from 30.8 kcal/mol for the unconstrained $Sn(OH)_3[OOC(OH)(CH_3)_2]$ intermediate to 29.3 kcal/mol for the constrained $Sn(OSiH_3)_3[OOC(OH)(CH_3)_2]$ intermediate. The rate-determining step for mechanism V remains the proton-transfer step. The value of ΔG_{total} for mechanism V is increased from 36.5 to 38.9 kcal/mol. This value of ΔG_{total} substantially exceeds the value calculated for mechanism IV using the constrained models, and mechanism V therefore still remains an unlikely pathway for tin-catalyzed Baeyer−Villiger oxidation.

The reactivity trends observed with the constrained, second coordination sphere cluster models are the same as those observed with the unconstrained, single coordination sphere cluster models. The similarity of the results support the usefulness of the minimal cluster model as a tool for accurately and rapidly predicting relative energetics of alternative reaction pathways.

Solvent Effects. The Baeyer−Villiger reactions modeled in this investigation occur under liquid-phase reaction conditions within the pores of a stannosilicate catalyst. To estimate possible effects of the polarizable reaction medium, we have recalculated the activation barriers for the Baeyer−Villiger rearrangement steps in mechanisms II, III, IV, and V using the IEF-PCM method[43] with highly polarizable methanol as solvent ($\epsilon = 32.63$). In the case of mechanism II, the activation barrier is slightly reduced from 35.7 kcal/mol in the gas phase to 35.0 kcal/mol in a methanol continuum. The activation barrier for rearrangement of the chelated Criegee intermediate C-1 in mechanisms III, IV, and V changes very little from 21.4 to 21.3 kcal/mol, while the activation barrier for intermediate C-2 is moderately reduced from 24.1 to 22.2 kcal/mol. Thus, the presence of a highly polarizable reaction medium reduces the relative difference between the activation barriers for the Criegee intermediate $Sn(OH)_3[OC(OOH)(CH_3)_2]$ with and without a water ligand on the tin center. The activation barrier for rearrangement of chelated Criegee intermediate C-3 to intermediate C-2 in mechanism V is slightly increased from 30.8 to 32.5 kcal/mol, so mechanism V is even less likely in a highly polarizable reaction medium. Additional IEF-PCM calculations show that Baeyer−Villiger rearrangement remains the rate-determining step of mechanisms III and IV in a methanol continuum.

Some effects of localized solvent coordination have been described above using water as a model solvent species. It has been shown that water molecules coordinating the tin active site facilitate proton transfer from hydrogen peroxide ligands and thereby lower the Gibbs activation barrier for tin hydroperoxo intermediate formation by 3−7 kcal/mol. A water ligand coordinating the tin center may also alter activation barriers for Criegee intermediate formation and rearrangement as discussed previously for mechanisms III, IV, and V. It is anticipated that protic solvent molecules may significantly influence reaction kinetics by facilitating proton-transfer steps in the various Baeyer−Villiger mechanisms.[38] Such solvent effects are beyond the scope of the present manuscript, but their importance certainly warrants future investigation.

Effect of Ketone Branching. It is generally found that increased branching of the migrating α carbon in the ketone substrate enhances reaction rates for Baeyer−Villiger oxidation with peroxycarboxylic acids.[1−4] Gavagnin et al.[17] have observed the same migratory preference for Baeyer−Villiger oxidation

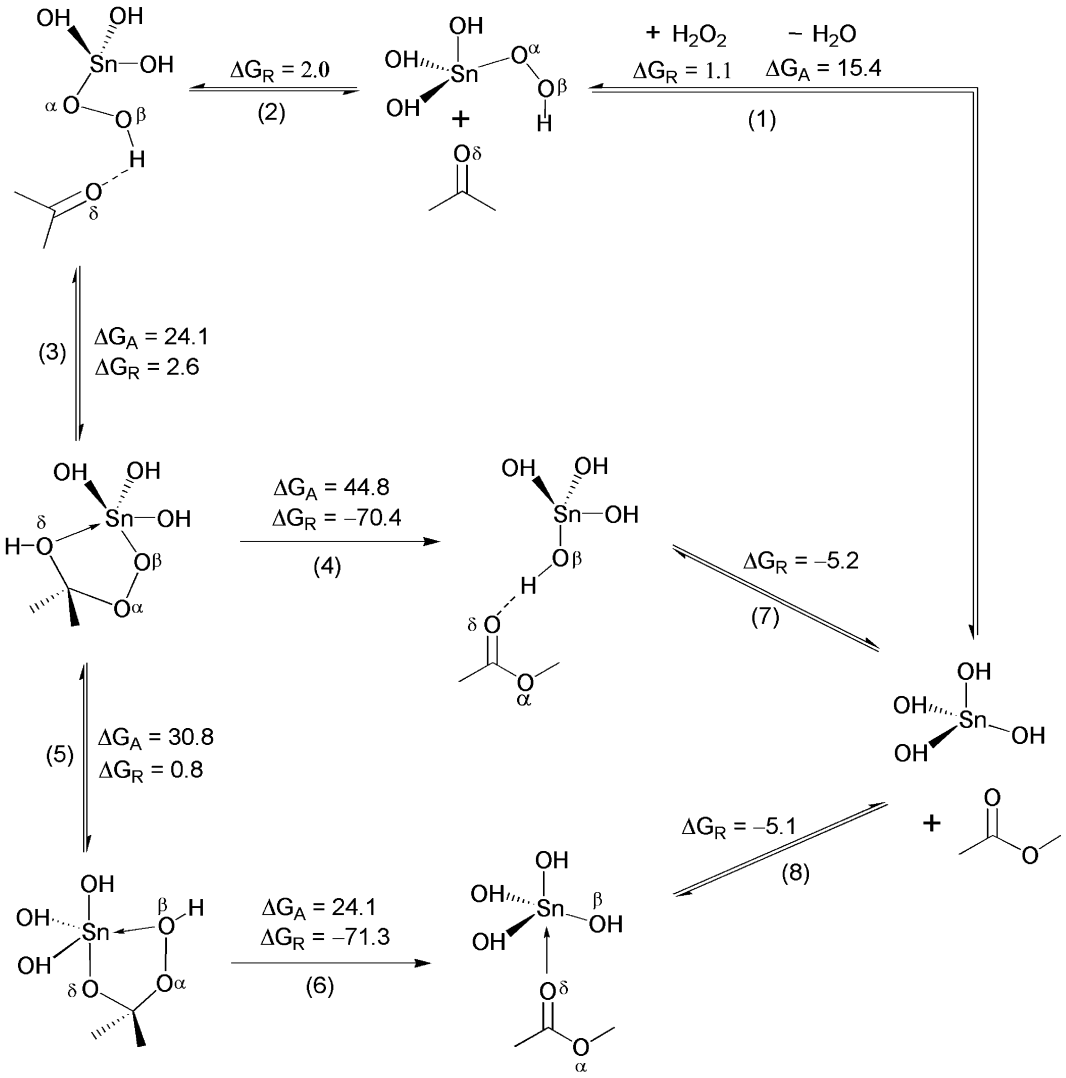

Figure 15. Mechanism V: tin-catalyzed Baeyer−Villiger oxidation of acetone with hydrogen peroxide. The tin hydroperoxo species acts like a peracid and adds across the carbonyl double bond of the noncoordinated acetone reactant. The structural arrows represent coordinative interactions with tin; dashed lines represent hydrogen-bonding interactions.

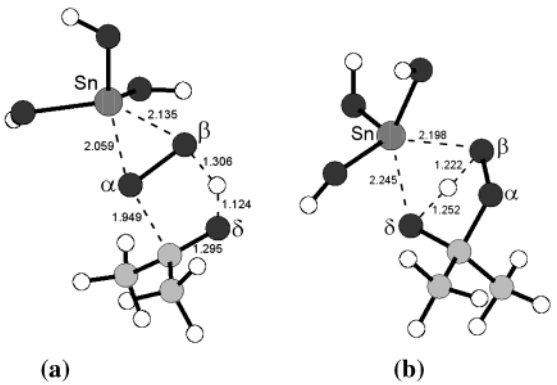

Figure 16. Optimized transition-state geometries for mechanism V: (a) addition of the tin hydroperoxo group across the carbonyl double bond of acetone via a five-membered ring (step 3); (b) intramolecular proton transfer to transform intermediate C-3 into C-2. Bonds in the process of breaking or forming are shown with dashed lines; bond distances are in Å.

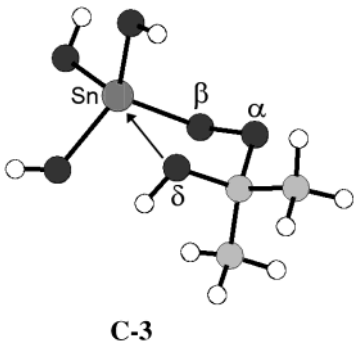

Figure 17. Optimized geometry of the chelated Criegee intermediate $Sn(OH)_3[OOC(OH)(CH_3)_2]$ or C-3.

of acyclic ketones with hydrogen peroxide using Pt^{II}(diphosphine) complexes as catalysts. Electron-donating alkyl groups on the migrating α carbon promote nucleophilic attack of the peroxo bond by stabilizing the developing positive charge on the migrating carbon in the Baeyer−Villiger rearrangement transition state. We have examined whether a similar effect occurs in the case of tin-catalyzed Baeyer−Villiger oxidation with hydrogen peroxide. The reaction energies and activation barriers for the Baeyer−Villiger oxidation of methyl isopropyl ketone and methyl *tert*-butyl ketone via steps 1−3, 6, and 9 of mechanism IV are compared with those for acetone in Table 5.

The energetics for steps 1 and 2 are the same for all three ketone substrates. As mentioned earlier, increased ketone

TABLE 5: Effect of Ketone Branching on Baeyer−Villiger Reaction Rate for Mechanism IV[a]

	$OC(CH_3)_2$		$OC(CH_3)[CH(CH_3)_2]$		$OC(CH_3)[C(CH_3)_3]$	
step	ΔG_R	ΔG_A	ΔG_R	ΔG_A	ΔG_R	ΔG_A
1	0.0	15.4	0.0	15.4	0.0	15.4
2	1.1		1.1		1.1	
3	2.3		−0.2		−2.8	
6	3.1	13.7	4.4	11.8	5.4	12.7
9	−71.3	24.1	−79.7	19.2	−81.9	16.5
ΔG_{total}[b]	30.6		24.5		20.2	

[a] All energies in kcal/mol. [b] ΔG_{total} defined as the sum of the Gibbs activation barrier for the rate-determining step and the Gibbs reaction energies for all preceding quasi-equilibrated steps.

branching augments the coordinative interaction between the carbonyl and the tin center (step 3). The activation barrier for attack of the proximal hydroperoxo oxygen Oα at the carbonyl carbon (step 6) changes little with increased ketone branching. As expected, the activation barrier for Baeyer−Villiger rearrangement decreases with increasing branching (step 9). The rate-determining step for all three ketones is the Baeyer−Villiger rearrangement. The relative reaction rates for each ketone can therefore be estimated with the same definition of ΔG_{total} used above for acetone; the values are reported in Table 5. The Baeyer−Villiger reaction rate clearly increases with increased ketone branching, and the $Sn(IV)-H_2O_2$ catalytic oxidation system therefore behaves similar to other Baeyer−Villiger oxidation systems.

No experimental data is available for the $Sn(IV)-H_2O_2$ catalytic oxidation system to compare with the calculated reactivity trends provided in Table 5. Only a crude, order-of-magnitude validation of the calculated branching effects can be obtained by comparison with experimental results from other Baeyer−Villiger oxidation systems. Hawthorne and Emmons[58] observed that phenyl *tert*-butyl ketone reacted about 20 times faster than isopropyl phenyl ketone with trifluoroperoxyacetic acid in ethylene chloride. Examination of graphical data reported by Gavagnin et al.[17] for their Pt^{II}(diphosphine) catalyst indicates that the initial reaction rate for Baeyer−Villiger oxidation of methyl *tert*-butyl ketone with hydrogen peroxide is about 20 times greater than that for methyl *sec*-butyl ketone in dichloroethylene. The difference in the activation barriers for tin-catalyzed Baeyer−Villiger rearrangement (step 9) approximately corresponds to a 100-fold greater intrinsic rate for methyl *tert*-butyl ketone compared to methyl isopropyl ketone. Thus, the computational results appear to demonstrate a reasonable order-of-magnitude.

Conclusions

Several possible reaction mechanisms for tin-catalyzed Baeyer−Villiger oxidation of acetone with hydrogen peroxide have been studied. The reaction most likely proceeds through a Criegee intermediate that contains a five-membered chelate ring with the tin center. Baeyer−Villiger rearrangement of the chelated Criegee intermediate is the rate-determining step for the overall reaction. The Gibbs activation barrier for rearrangement of the chelated Criegee intermediate is over 17 kcal/mol less than the corresponding activation barrier for the nonchelated Criegee intermediate in the noncatalyzed mechanism. The Lewis acidic tin center facilitates the rearrangement step by stabilizing the hydroxyl leaving group as the peroxo bond is cleaved in the transition state. Two degenerate pathways exist for the formation of the chelated Criegee intermediate; both pathways require combined interaction of the ketone substrate and the hydrogen peroxide oxidant with the tin active site. It has been clearly demonstrated that a mechanism in which tin activates the ketone carbonyl for reaction with free hydrogen peroxide cannot explain the rate enhancements achieved with tin-containing redox molecular sieve catalysts. Electron-donating alkyl groups on the migrating α carbon in the ketone substrate reduce the activation barrier for the rate-determining rearrangement step by promoting nucleophilic attack of the peroxo bond. As this computational study is the first to consider metal-catalyzed Baeyer−Villiger reaction chemistry, it is hoped that the results presented here will not only benefit future research into tin-based catalysts but also help guide the development of alternative catalytic systems.

Acknowledgment. We gratefully acknowledge the financial support of the National Science Foundation Training Grant (DGE−9554586) for the program "Catalysis for Environmentally Conscious Manufacturing" and funding received through a National Science Foundation Fellowship (R.R.S.). We also thank Dr. Frank A. Weinhold for helpful discussions.

References and Notes

(1) Bolm, C. *Adv. Catal. Processes* **1997**, *2*, 43−68.
(2) Krow, G. R. *Org. React.* **1993**, *43*, 251−798.
(3) Renz, M.; Meunier, B. *Eur. J. Org. Chem.* **1999**, 737−750.
(4) Strukul, G. *Angew. Chem., Int. Ed. Engl.* **1998**, *37*, 1198−1209.
(5) Campestrini, S.; Di Furia, F. *J. Mol. Catal.* **1993**, *79*, 13−19.
(6) Sato, K.; Hyodo, M.; Takagi, J.; Aoki, M.; Noyori, R. *Tetrahedron Lett.* **2000**, *41*, 1439−1442.
(7) ten Brink, G.-J.; Vis, J.-M.; Arends, I. W. C. E.; Sheldon, R. A. *J. Org. Chem.* **2001**, *66*, 2429−2433.
(8) Fischer, J.; Hölderich, W. F. *App. Catal. A: Gen.* **1999**, *180*, 435−443.
(9) Jacobson, S. E.; Mares, F.; Zambri, P. M. *J. Am. Chem. Soc.* **1979**, *101*, 6938−6946.
(10) Lambert, A.; Macquarrie, D. J.; Carr, G.; Clark, J. H. *New J. Chem.* **2000**, *24*, 485−488.
(11) Taylor, R. T.; Flood, L. A. *J. Org. Chem.* **1983**, *48*, 5160−5164.
(12) Wang, Z. B.; Mizusaki, T.; Sano, T.; Kawakami, Y. *Bull. Chem. Soc. Jpn.* **1997**, *70*, 2567−2570.
(13) Walsh, C. T.; Chen, Y.-C. J. *Angew. Chem., Int. Ed. Engl.* **1988**, *27*, 333−343.
(14) Mazzini, C.; Lebreton, J.; Furstoss, R. *J. Org. Chem.* **1996**, *61*, 8−9.
(15) Murahashi, S.-I.; Ono, S.; Imada, Y. *Angew. Chem., Int. Ed.* **2002**, *41*, 2366−2368.
(16) Frisone, M. D. T.; Pinna, F.; Strukul, G. *Organometallics* **1993**, *12*, 148−156.
(17) Gavagnin, R.; Cataldo, M.; Pinna, F.; Strukul, G. *Organometallics* **1998**, *17*, 661−667.
(18) Strukul, G.; Varagnolo, A.; Pinna, F. *J. Mol. Catal. A: Chem.* **1997**, *117*, 413−423.
(19) Herrmann, W. A.; Fischer, R. W.; Correia, J. D. G. *J. Mol. Catal.* **1994**, *94*, 213−223.
(20) Phillips, A. M. F.; Romão, C. *Eur. J. Org. Chem.* **1999**, 1767−1770.
(21) Uchida, T.; Katsuki, T. *Tetrahedron Lett.* **2001**, *42*, 6911−6914.
(22) Watanabe, A.; Uchida, T.; Ito, K.; Katsuki, T. *Tetrahedron Lett.* **2002**, *43*, 4481−4485.
(23) Palazzi, C.; Pinna, F.; Strukul, G. *J. Mol. Catal. A: Chem.* **2000**, *151*, 245−252.
(24) Bhaumik, A.; Kumar, P.; Kumar, R. *Catal. Lett.* **1996**, *40*, 47−50.
(25) Corma, A.; Nemeth, L. T.; Renz, M.; Valencia, S. *Nature* **2001**, *412*, 423−425.
(26) Renz, M.; Blasco, T.; Corma, A.; Fornés, V.; Jensen, R.; Nemeth, L. *Chem. Eur. J.* **2002**, *8*, 4708−4717.
(27) Corma, A.; Navarro, M. T.; Nemeth, L.; Renz, M. *Chem. Commun.* **2001**, 2190−2191.
(28) Pillai, U. R.; Sahle-Demessie, E. *J. Mol. Catal. A: Chem.* **2003**, *191*, 93−100.
(29) Berkesel, A.; Andreae, M. R. M. *Tetrahedron Lett.* **2001**, *42*, 2293−2295.
(30) Matsumoto, M.; Kobayashi, H. *Heterocycles* **1986**, *24*, 2443−2447.
(31) McClure, J. D.; Williams, P. H. *J. Org. Chem.* **1962**, *27*, 24−26.
(32) Neimann, K.; Neumann, R. *Org. Lett.* **2000**, *2*, 2861−2863.
(33) Cárdenas, R.; Cetina, R.; Lagúnez-Otero, J.; Reyes, L. *J. Phys. Chem. A* **1997**, *101*, 192−200.
(34) Cárdenas, R.; Reyes, L.; Lagúnez-Otero, J.; Cetina, R. *THEOCHEM* **2000**, *497*, 211−225.

(35) Hannachi, H.; Anoune, N.; Arnaud, C.; Lantéri, P.; Longeray, R.; Chermette, H. *THEOCHEM* **1998**, *434*, 183−191.
(36) Lehtinen, C.; Nevalainen, V.; Brunow, G. *Tetrahedron* **2000**, *56*, 9375−9382.
(37) Lehtinen, C.; Nevalainen, V.; Brunow, G. *Tetrahedron* **2001**, *57*, 4741−4751.
(38) Okuno, Y. *Chem. Eur. J.* **1997**, *3*, 212−218.
(39) Stoute, V. A.; Winnik, M. A.; Csizmadia, I. G. *J. Am. Chem. Soc.* **1974**, *96*, 6388−6393.
(40) Carlqvist, P.; Eklund, R.; Brinck, T. *J. Org. Chem.* **2001**, *66*, 1193−1199.
(41) Frisch, M. J.; Trucks, G. W.; Schlegel, H. B.; Scuseria, G. E.; Robb, M. A.; Cheeseman, J. R.; Zakrzewski, V. G.; Montgomery, J. A., Jr.; Stratmann, R. E.; Burant, J. C.; Dapprich, S.; Millam, J. M.; Daniels, A. D.; Kudin, K. N.; Strain, M. C.; Farkas, O.; Tomasi, J.; Barone, V.; Cossi, M.; Cammi, R.; Mennucci, B.; Pomelli, C.; Adamo, C.; Clifford, S.; Ochterski, J.; Petersson, G. A.; Ayala, P. Y.; Cui, Q.; Morokuma, K.; Malick, D. K.; Rabuck, A. D.; Raghavachari, K.; Foresman, J. B.; Cioslowski, J.; Ortiz, J. V.; Stefanov, B. B.; Liu, G.; Liashenko, A.; Piskorz, P.; Komaromi, I.; Gomperts, R.; Martin, R. L.; Fox, D. J.; Keith, T.; Al-Laham, M. A.; Peng, C. Y.; Nanayakkara, A.; Gonzalez, C.; Challacombe, M.; Gill, P. M. W.; Johnson, B. G.; Chen, W.; Wong, M. W.; Andres, J. L.; Head-Gordon, M.; Replogle, E. S.; Pople, J. A. *Gaussian 98*, revision A.9; Gaussian, Inc.: Pittsburgh, PA, 1998.
(42) Glendening, E. D.; Badenhoop, J. K.; Reed, A. E.; Carpenter, J. E.; Bohmann, J. A.; Morales, C. M.; Weinhold, F. NBO 5.0. Theoretical Chemistry Institute: University of Wisconsin, Madison, WI, 2001.
(43) Cancès, E.; Mennucci, B.; Tomasi, J. *J. Chem. Phys.* **1997**, *107*, 3032−3041.
(44) Check, C. E.; Faust, T. O.; Bailey, J. M.; Wright, B. J.; Gilbert, T. M.; Sunderlin, L. S. *J. Phys. Chem. A* **2001**, *105*, 8111−8116.
(45) Weinhold, F. A. In *Encyclopedia of Computational Chemistry*; Schleyer, P. v. R., Ed.; John Wiley & Sons: New York, 1998.
(46) Chaudhari, K.; Das, T. K.; Rajmohanan, P. R.; Lazar, K.; Sivasanker, S.; Chandwadkar, A. J. *J. Catal.* **1999**, *183*, 281−291.
(47) Lázár, K.; Szeleczky, A. M.; Mal, N. K.; Ramaswamy, A. V. *Zeolites* **1997**, *19*, 123−127.
(48) Mal, N. K.; Ramaswamy, V.; Rajamohanan, P. R.; Ramaswamy, A. V. *Micropor. Mater.* **1997**, *12*, 331−340.
(49) Mal, N. K.; Ramaswamy, A. V. *J. Mol. Catal. A: Chem.* **1996**, *105*, 149−158.
(50) Mal, N. K.; Bhaumik, A.; Kumar, R.; Ramaswamy, A. V. *Catal. Lett.* **1995**, *33*, 387−394.
(51) Mal, N. K.; Ramaswamy, V.; Ganapathy, S.; Ramaswamy, A. V. *Chem. Commun.* **1994**, 1933−1934.
(52) Gonzalez, C.; Schlegel, H. B. *J. Chem. Phys.* **1989**, *90*, 2154−2161.
(53) van Koningsveld, H.; Jansen, J. C.; van Bekkum, H. *Zeolites* **1990**, *10*, 235−242.
(54) Sever, R. R.; Root, T. W. *J. Phys. Chem. B* **2003**, *107*, 4080−4089.
(55) Mal, N. K.; Ramaswamy, A. V. *Chem. Commun.* **1997**, 425−426.
(56) Mal, N. K.; Ramaswamy, V.; Rakshe, B.; Ramaswamy, A. V. *Stud. Surf. Sci. Catal.* **1997**, *105*, 357−364.
(57) Mal, N. K.; Bhaumik, A.; Ramaswamy, V.; Belhekar, A. A.; Ramaswamy, A. V. *Stud. Surf. Sci. Catal.* **1995**, *94*, 317−324.
(58) Hawthorne, M. F.; Emmons, W. D.; McCallum, K. S. *J. Am. Chem. Soc.* **1958**, *80*, 6393−6398.